Mon. Not. R. Astron. Soc. **000**, 000–000 (0000) Printed 13 March 2012 (MN LATEX style file v2.2)

Evolution of luminosity function and obscuration of AGN: connecting X-ray and Infrared

Yunkun Han[1,2,3⋆], Benzhong Dai[4], Bo Wang[1,3], Fenghui Zhang[1,3], Zhanwen Han[1,3]
[1]*National Astronomical Observatories/Yunnan Observatory, the Chinese Academy of Sciences, Kunming 650011, China*
[2]*Graduate University of Chinese Academy of Sciences, Beijing 100049, China*
[3]*Key Laboratory for the Structure and Evolution of Celestial Objects, the Chinese Academy of Sciences, Kunming 650011, China*
[4]*Department of Physics, Yunnan University, Kunming 650091, China*

Accepted 2012 March 8. Received 2012 March 6; in original form 2010 September 6

ABSTRACT

We present a detailed comparison between the $2-10$ keV hard X-ray and infrared (IR) luminosity function (LF) of active galactic nuclei (AGN). The composite X-ray to IR spectral energy distributions (SEDs) of AGN used for connecting the hard X-ray LF (HXLF) and IR LF (IRLF) are modeled with a simple but well tested torus model based on the radiative transfer and photoionization code CLOUDY. Four observational determinations of the evolution of $2-10$ keV HXLF and six evolution models of the obscured type-2 AGN fraction (f_2) have been considered. The 8.0 and 15 μm LFs for the total, unobscured type-1 and obscured type-2 AGN are predicted from the HXLFs, and then compared with the measurements currently available. We find that the IRLFs predicted from HXLFs tend to underestimate the number of the most IR-luminous AGN. This is independent of the choices of HXLF and f_2, and even more obvious for the HXLFs recently measured. We show that the discrepancy between the HXLFs and IRLFs can be largely resolved when the anticorrelation between the UV to X-ray slope $\alpha_{\rm ox}$ and UV luminosity $L_{\rm UV}$ is appropriately considered. We also discuss other possible explanations for the discrepancy, such as the missing population of Compton-thick AGN and possible contribution of star-formation in the host to the mid-IR. Meanwhile, we find that the HXLFs and IRLFs of AGN can be more consistent with each other if the obscuration mechanisms of quasars and Seyferts are assumed to be different, corresponding to their different triggering and fueling mechanisms. More accurate measurements of the IRLFs of AGN, especially that determined at smaller redshift bins and more accurately separated to that for type-1 and type-2, are very helpful for clarifying these interesting issues.

Key words: galaxies: active – galaxies: luminosity function – galaxies: formation – galaxies: evolution – infrared: galaxies – X-rays: galaxies

1 INTRODUCTION

Active galactic nucleus (AGN), compact regions at the center of active galaxies, releasing a great deal of energies in the form of radiation over the electromagnetic spectrum from radio, infrared, optical, ultraviolet, X-ray to γ-ray, are now believed to be powered by accretion of mass into the super-massive black holes (SMBHs). In the local Universe, SMBHs are found to exist at the center of most massive galaxies. There are good correlations between the mass of SMBHs and the properties of host galaxies (Hopkins et al. 2007; Kormendy & Bender 2009; Gültekin et al. 2009; Merloni et al. 2010), such as the velocity dispersion (Ferrarese & Merritt 2000; Gebhardt et al. 2000; Tremaine et al. 2002), mass (Magorrian et al. 1998; Häring & Rix 2004; Graham 2004), or luminosity (Kormendy & Richstone 1995; Marconi & Hunt 2003) of host bulge. On the other hand, the AGN activity and star formation are found to peak at a similar redshift and decline towards low redshift simultaneously (Hopkins 2004; Silverman et al. 2008; Aird et al. 2010). Meanwhile, the mass density of local SMBHs in galaxy center is found to be consistent with that accreted by AGN throughout the history of the Universe (Marconi et al. 2004; Merloni 2004). These correlations strongly support the idea that the growth of SMBHs should be coupled with the formation and evolution of galaxies (Croton et al. 2006; Bower et al. 2006; Di Matteo et al. 2005, 2008; Hopkins et al. 2005, 2006, 2008), although some authors (e.g. Peng 2007; Jahnke & Macciò 2011) argued a non-causal origin of them.

While the important role of SMBHs, and so AGN, playing in the formation and evolution of galaxies has been well established, detailed mechanisms about this process are still largely unknown. The luminosity functions (LF) of AGN, which de-

⋆ E-mail: hanyk@ynao.ac.cn

scribe the spacial density of AGN as a function of luminosity and redshift, is an important observable quantity for understanding the distribution and evolution of AGN. It constrains the accretion history of SMBHs, and reveals the triggering and fueling mechanism of AGN and their co-evolution with host galaxies. An observational determination of the bolometric LFs of AGN require multi-wavelength observations spanning the whole wavelength range of electromagnetic spectrum and sampling large comoving volume and luminosity range. So, in practice, the LFs of AGN are measured independently from different wavelength bands such as radio (e.g. Nagar et al. 2005), infrared (e.g. Babbedge et al. 2006; Brown et al. 2006; Matute et al. 2006), optical (e.g. Fan et al. 2001; Wolf et al. 2003; Croom et al. 2004; Richards et al. 2006; Bongiorno et al. 2007; Fontanot et al. 2007; Shankar & Mathur 2007), soft X-ray (e.g. Miyaji et al. 2000, 2001; Silverman et al. 2005a; Hasinger et al. 2005), hard X-ray (e.g. Ueda et al. 2003; La Franca et al. 2005; Silverman et al. 2005b, 2008; Yencho et al. 2009; Ebrero et al. 2009; Aird et al. 2010), or emission lines (e.g. Hao et al. 2005). However, due to the different selection effect suffered by different bands, the LFs of AGN measured from different bands are not necessarily consistent with each other.

Among various bands, X-ray, especially the hard X-ray band, is the most efficient for selecting AGN. Recently, the evolution of the hard X-ray LF (HXLF) of AGN from $z \sim 0$ to 5 is found to be best described by a luminosity dependent density evolution (LDDE) model. According to this model, the spatial density of AGN with lower luminosity peaked at lower redshift than those with high luminosity, and the faint-end slope of the LFs is flattened as redshift increased (Ueda et al. 2003; Barger et al. 2005; Hasinger et al. 2005). This kind of so-called 'cosmic downsizing' evolution trend of the AGN population has been further confirmed in radio and optical bands (Cirasuolo et al. 2005; Bongiorno et al. 2007). These results revealed a dramatically different evolutionary model for Seyfert galaxies and quasars, and imply very different triggering, fueling and accretion mechanisms for the two classes of AGN.

Meanwhile, AGN are classified to two major classes according to their optical spectra. Type-1 AGN exhibits both broad permitted lines and narrow forbidden lines in their spectra, while type-2 AGN presents only the narrow lines (Khachikian & Weedman 1974). Rowan-Robinson (1977) firstly put forward the idea that AGN are surrounded by dusty medium which absorbs their visible and ultraviolet light and then re-emits them in the mid-IR. The extinction due to these obscuring medium is responsible for the distinction between type-1 and type-2 AGN. Latterly, this idea was developed into the so-called unified model of AGN (Pier & Krolik 1992; Antonucci 1993; Maiolino & Rieke 1995; Krolik 1999; Zhang & Wang 2006; Wang & Zhang 2007). In the model, the differences between different types of AGN can be explained by the anisotropically distributed obscuring mediums (often visualized as a geometrically and optically thick torus comprised of dust and molecular gas) surrounding a basic black hole-accretion disk system, while different lines-of-sight into and through these obscuring mediums result in the diverse observational properties of AGN population.

However, the obscuration of AGN by anisotropically distributed gas/dust medium imply great systematic selection bias for understanding the properties and evolution of AGN. Moreover, obscuring mediums around AGN are recently found to be distributed in a much more complex manner than a simple compact torus (Risaliti et al. 2002; Kuraszkiewicz et al. 2003; Risaliti et al. 2005; Goulding & Alexander 2009), and may evolve with luminosity (Ueda et al. 2003; Steffen et al. 2003; Hasinger 2004; Barger et al. 2005; Simpson 2005) and redshift (La Franca et al. 2005; Ballantyne et al. 2006a; Treister & Urry 2006; Hasinger 2008; Ebrero et al. 2009). These results imply that the observational properties of AGN may vary significantly from object to object. This complicates the understanding of the intrinsic characteristics of AGN and their correlations with the host galaxy. On the other hand, current state-of-art synthesis models of cosmic X-ray background (CXRB) (e.g. Gilli et al. 2007) show that a large population of heavily obscured Compton-thick AGN (with $N_{\rm H} \leqslant 10^{24}{\rm cm}^{-2}$) are required to fit the CXRB spectrum. This population of Compton-thick AGN can be missed by even the deep hard X-ray surveys since they are deeply buried by obscuring medium.

Furthermore, recent results of Hasinger (2008) and Treister et al. (2010) show that the fraction of absorbed AGN increases significantly with redshift to $z \sim 2-3$, accompanied with the cosmic co-evolution of star-formation and AGN activity. These results support the idea that the obscuration of AGN cannot simply come from an unevolving torus employed by traditional unified model of AGN. The obscuration mechanism of AGN with different triggering, fueling and accretion mechanisms may be different and associated with their co-evolution with galaxies (Davies et al. 2006; Ballantyne et al. 2006a; Ballantyne 2008).

So, detailed studies of the obscuring medium around AGN, such as their geometry, distribution, composition, origin, and evolution, are very important (Zhang 2004; Wang et al. 2005; Liu & Zhang 2011). The obscured or absorbed optical, ultraviolet, and X-ray radiation will be re-emitted in the infrared (IR). IR bands represent an important complement for understanding the properties of obscuring medium around AGN and their co-evolution with host galaxies. With the existing IR space telescope such as *Spitzer*, *Herschel* and forthcoming *James Webb Space Telescope (JWST)*, our observation and understanding of AGN from the IR band will be largely improved. Given the limitations suffered by X-ray observations, it is important to study the LFs and obscuration of AGN together and test the conclusions about their evolution, which are mainly based on observations in the X-ray band, in the IR band.

By using the spectral energy distributions (SEDs) modeled with a simple torus model, which is based on the radiative transfer and photoionization code CLOUDY, Ballantyne et al. (2006b) can relate the X-ray and IR properties of AGN and explore the effects of parameters about obscuring medium. They presented the mid-IR number counts and LFs for three evolution models of the f_2 (equal to the covering factor under the unified model of AGN) that are constrained by the synthesis model of CXRB. The mid-IR number counts and LFs predicted from HXLF are in good agreement with direct IR observations, especially when assuming an inner radius ($R_{\rm in}$) of $10\ {\rm pc}$ for the obscuring medium as expected if the obscuring material is connected to galactic-scale phenomenon. The mid-IR LFs of AGN are found to be a much better tool for determining the evolution of f_2 with z.

Ballantyne et al. (2006b) presented the mid-IR LFs for total AGN at different redshifts, but the observational mid-IR LFs of AGN (i.e. Brown et al. 2006), which is used to be compared with, are for type-1 AGN only. After the work of Ballantyne et al. (2006b), some important improvements to the measurement of HXLF of AGN have been presented (e.g. Silverman et al. 2008; Ebrero et al. 2009; Aird et al. 2010). Furthermore, the actual evolution model of AGN obscuration is not necessarily within the three models proposed by Ballantyne et al. (2006a), other possibilities need to be tested for more reasonable conclusions.

In this paper, we present a more detailed comparison between the HXLFs and mid-IR LFs of AGN, which are connected by the composite X-ray to IR SEDs modeled with a modified version of the simple by well tested torus model of Ballantyne et al. (2006b). More observational determinations of the $2-10$ keV HXLF and the evolution models of f_2 have been considered. The 8.0 and 15 μm LF for the total, unobscured type-1 and obscured type-2 AGN are predicted from different combinations of HXLF and f_2, and then compared with current IR observational results. Besides the measurement of Brown et al. (2006), the 15 μm LF given by Matute et al. (2006) and recent results of Fu et al. (2010) have been added for comparison.

We begin in Section 2 by reviewing current understanding of AGN evolution from X-ray band. This include current observational determination of the evolution of the HXLF of AGN in Section 2.1, and the evolution of AGN obscuration in Section 2.2. The detailed procedures of modeling the composite X-ray to IR SED of AGN, and our modifications to the original torus model of Ballantyne et al. (2006b), are presented in Section 3. Section 4 presents the method used to compute the IRLFs of type-1, type-2 and total AGN from different combinations of HXLF and f_2. In Section 5, we present our results and compare them with measurements from direct mid-IR observations to seek conclusions about the evolution of LFs and obscuration of AGN from combined views of hard X-ray and mid-IR. We find that the mid-IR LFs predicted from HXLFs tend to underestimate the number of the most IR-luminous AGN, which is independent of the choices of HXLF and f_2, and even more obvious for the HXLFs recently determined. In Section 6, we discuss explanations for this. Finally, a summary of this paper is presented in Section 7.

Throughout this paper, we adopt a $H_0 = 70$ km s^{-1} Mpc^{-1}, $\Omega_\Lambda = 0.7$, and $\Omega_m = 0.3$ (Spergel et al. 2003) cosmology. Minor differences in the cosmology have negligible effects on our conclusions.

2 THE EVOLUTION OF AGN REVEALED FROM X-RAY BANDS

2.1 The evolution of the HXLF of AGN

Strong X-ray emission is a unique indication of an AGN activity at the center of galaxies. Deep X-ray surveys by *Chandra* and *XMM-Newton*, which have already resolved most of the $2-10$ keV cosmic X-ray background (CXRB) into individual sources, found that most sources of CXRB are AGN. X-ray, especially hard X-ray with energy $\geqslant$2 keV, are highly efficient for selecting AGN. Both the moderately obscured ($N_{\rm H} \leqslant 10^{23}$ cm^{-2}) and low-luminosity sources commonly missed by optical observations can be selected from hard X-ray. So, much more trustable evolution trends of the AGN can be revealed from hard X-ray observations.

As mentioned above, HXLF of AGN is found to be best described by a LDDE model. However, the exact form of the evolution is still under debate, especially at high redshifts. In this paper, we adopt the LDDE model given by Ueda et al. (2003), where the present-day HXLF is described as a smoothly-connected double power-law form:

$$\frac{{\rm d}\Phi(L_{\rm X}, z=0)}{{\rm dlog}L_{\rm X}} = {\rm A}[(L_{\rm X}/L_*)^{\gamma 1} + (L_{\rm X}/L_*)^{\gamma 2}]^{-1}, \quad (1)$$

where $\gamma 1$ is faint-end slope, $\gamma 2$ is the bright-end slope, L_* is the characteristic break luminosity and A is a normalisation factor. The

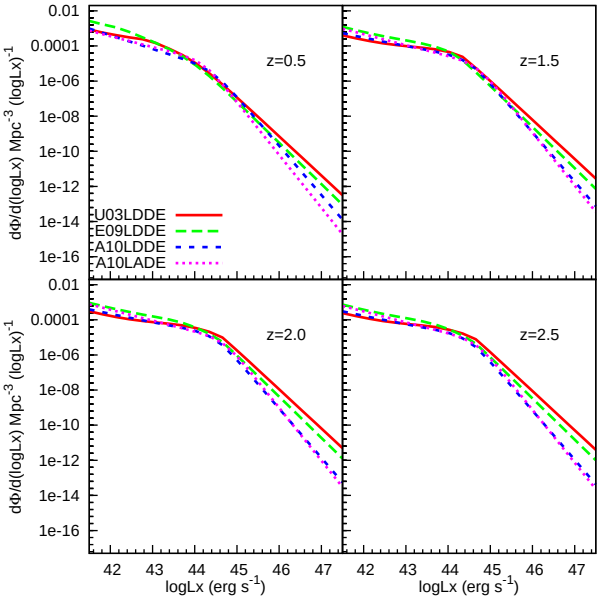

Figure 1. HXLF of AGN at $z = 0.5, 1.5, 2.0$ and 2.5 as given by the LDDE model of Ueda et al. (2003) (red solid line, noted as U03LDDE), Ebrero et al. (2009) (green dashed line, noted as E09LDDE), Aird et al. (2010) (blue short dashed line, noted as A10LDDE) and the LADE model of Aird et al. (2010) (purple dot line, noted as A10LADE), respectively.

evolution of LFs is given by

$$\frac{{\rm d}\Phi(L_{\rm X}, z)}{{\rm dlog}L_{\rm X}} = \frac{{\rm d}\Phi(L_{\rm X}, 0)}{{\rm dlog}L_{\rm X}} e(z, L_{\rm X}), \quad (2)$$

where the evolution term is given by

$$e(z, L_{\rm X}) = \begin{cases} (1+z)^{p1} & [z < z_{\rm c}(L_{\rm X})] \\ e(z_{\rm c})[\frac{1+z}{1+z_{\rm c}(L_{\rm X})}]^{p2} & [z \geqslant z_{\rm c}(L_{\rm X})]. \end{cases} \quad (3)$$

The cutoff redshift $z_{\rm c}$, with a dependence on the luminosity starting from a characteristic luminosity L_a, are given by a power law of $L_{\rm X}$:

$$z_{\rm c}(L_{\rm X}) = \begin{cases} z_{\rm c}^* & (L_{\rm X} \geqslant L_a) \\ z_{\rm c}^* \left(\frac{L_{\rm X}}{L_a}\right)^{\alpha} & (L_{\rm X} < L_a), \end{cases} \quad (4)$$

where α measures the strength of the dependence of $z_{\rm c}$ with luminosity.

Recently, Ebrero et al. (2009) re-measured the HXLF of AGN by using the *XMM-Newton* Medium Survey (XMS, Barcons et al. 2007) and other highly complete deeper and shallower surveys to assemble an overall sample of ~ 450 identified AGN in the $2-10$ keV band, which is one of the largest and most complete sample up to date. Aird et al. (2010) presented a new observational determination of the evolution of the $2-10$ keV HXLF of AGN by using data from many surveys including 2 Ms *Chandra* Deep Fields and the AEGIS-X 200 ks survey. These, combined with a sophisticated Bayesian methodology, allow them to do a more accurate measurement of the evolution of the faint end of the HXLF. They found that the evolution of HXLF are best described by a so called luminosity and density evolution (LADE) model, rather than the LDDE model. The LADE model is a modified Pure luminosity evolution (PLE) model. According to the PLE model (Ueda et al. 2003), the evolution of HXLF with redshift are described by allowing the charac-

teristic break luminosity L_* in the present-day HXLF as given by Eq. (1) to evolve as

$$\log L_*(z) = \log L_0 - \log\left[\left(\frac{1+z_c}{1+z}\right)^{p_1} + \left(\frac{1+z_c}{1+z}\right)^{p_2}\right] \quad (5)$$

where the parameter z_c controls the transition from the strong low-z evolution to the high-z form. The LADE model are constructed by additionally allowing for overall decreasing density evolution with redshift, i.e. allowing the normalization constant A in the present-day HXLF as given by Eq. (1) to evolve as

$$\log A(z) = \log \mathrm{A}_0 + \mathrm{d}(1+z) \quad (6)$$

where d is an additional parameter describing the overall density decreasing.

In Fig. 1, we show the HXLF of AGN at $z = 0.5, 1.5, 2.0$ and 2.5 as given by the LDDE model of Ueda et al. (2003), Ebrero et al. (2009), Aird et al. (2010), and the LADE model of Aird et al. (2010). The LADE modeling of the HXLF retains the same shape at all redshifts, but undergoes strong luminosity evolution out to $z \sim 1$. Meanwhile, the HXLF undergoes overall negative density evolution with increasing redshift. Fig. 1 clearly shows that the HXLF of Aird et al. (2010) is different from those of the others at high luminosity.

Different HXLFs have very different implications for the AGN populations, such as their lifetimes, duty cycles, fueling, triggering and evolution. Further complemental views from other wavelength bands, such as IR, are important for a fully understanding of the evolution of AGN populations. In this paper, the four modelings of HLXF mentioned above have been used to predict the evolution of mid-IR LFs of type-1 and/or type-2 AGN, respectively.

2.2 The evolution of the obscuration of AGN

Since there is a good correspondence between the AGN with $N_{\rm H} \geqslant 10^{22}$ cm^{-2} and those optically identified as being of type-2 (Tozzi et al. 2006), type-2 AGN is commonly defined as those with absorbing column densities $N_{\rm H} \geqslant 10^{22}$ cm^{-2} in the X-ray band. According to the unified model of AGN, f_2 approximately equal to the covering factor of the gas with $N_{\rm H} \geqslant 10^{22}$ cm^{-2} around the AGN.

By using a population synthesis model of CXRB, Ballantyne et al. (2006a) constrained the evolution of f_2 as a function of both z and $L_{\rm X}$. They presented three parameterizations for the evolution of $f_2(\log L_X, z)$ that could fit the observed shape of the CXRB and X-ray number counts of AGN. The first one (shown in Fig. 2, and noted as 'f2_1'), with a moderate redshift evolution, is given as:

$$f_2 = \mathrm{K}_1(1+z)^{0.3}(\log L_{\rm X})^{-4.8}, \quad (7)$$

where K_1 is a constant defined by $f_2(\log L_{\rm X} = 41.5, z = 0) = 0.8$, which is based on observations in the local Universe. The second one (shown in Fig. 2, and noted as 'f2_2') with a more rapid redshift evolution, is given as:

$$f_2 = \mathrm{K}_2(1+z)^{0.9}(\log L_{\rm X})^{-1.3}, \quad (8)$$

where K_2 is based on the Sloan Digital Sky Survey (SDSS) measurement of $f_2(\log L_{\rm X} = 41.5, z = 0) = 0.5$ by Hao et al. (2005). In the above two cases, the z evolution is halted at $z = 1$, because there is no constraint on f_2 at higher redshifts. The last one (shown in Fig. 2, and noted as 'f2_3'), which is considered as a null-hypothesis, assumes that f_2 does not evolve with redshift, and given as:

$$f_2 = \mathrm{K}_3 \cos^2\left(\frac{\log L_{\rm X} - 41.5}{9.7}\right), \quad (9)$$

where K_3 is determined by $f_2(\log L_{\rm X} = 41.5, z = 0) = 0.8$.

The fraction of type-2 AGN can also be measured directly from observations in different bands. For example, in the optical, AGN can be selected using their high ionization lines to construct the standard diagnostic diagrams (Baldwin et al. 1981; Kewley et al. 2001; Kauffmann et al. 2003; Kewley et al. 2006). Furthermore, the ratio of narrow-line and broad-line AGN can be measured as a function of z and the luminosity of emission lines (such as [O III] 5007Å line), which can be used as AGN power indicators. However, significant limitations of optical selection and classification of AGN have been noticed (e.g. Moran et al. 2002; Netzer et al. 2006; Rigby et al. 2006). The nuclear emission can be obscured by the torus and/or outshone by the host-galaxy light. Alternatively, AGN can be efficiently selected in the X-ray, and the X-ray luminous AGN can be classified to absorbed and unabsorbed according to their absorbing column densities $\log N_{\rm H} < 22$ or > 22. X-ray selection of AGN is suffered by the limited sensitivity of telescopes, which are only sensitive at $\leqslant 10$ keV. So, a significant fraction of absorbed objects, especially the large number of Compton-thick AGN with $\log N_{\rm H} > 24$ predicted by the population synthesis model of CXRB, may be missed by current hard X-ray selection of AGN.

The combination of X-ray and optical criteria is a much more robust method for the selection and classification of AGN. Recently, Hasinger (2008) have presented a new determination of the fraction of absorbed sources as a function of X-ray luminosity and redshift from a sample of 1290 AGN. They are selected in the $2-10$ keV band from different flux-limited surveys with very high optical identification completeness, and grouped into type-1 and type-2 according to their optical spectroscopic classification and X-ray absorption properties. So, the evolution of AGN absorption with luminosity and redshift is determined with higher statistical accuracy and smaller systematic errors than previous results. The absorbed fraction is found to decrease strongly with X-ray luminosity, and can be represented by an almost linear decrease with a slope of 0.281 ± 0.016. Meanwhile, it increase significantly with redshift as $\sim (1+z)^{0.62\pm0.11}$ from $z = 0$ to $z \sim 2$. On the other hand, the evolution of the absorbed AGN fraction over the whole redshift from $z = 0$ to $z \sim 5$ can also be described as $\sim (1+z)^{0.48\pm0.08}$, or $\sim (1+z)^{0.38\pm0.09}$ when data with crude redshifts are excluded.

These findings may have important consequences for the broader context of AGN and galaxy co-evolution. According to the results of Hasinger (2008), we have constructed three new evolution models of AGN obscuration, which are expressed as

$$f_2 = -0.281(\log L_{\rm X} - 43.75) + 0.279(1+z)^{0.62}, \quad (10)$$

$$f_2 = -0.281(\log L_{\rm X} - 43.75) + 0.308(1+z)^{0.48}, \quad (11)$$

$$f_2 = -0.281(\log L_{\rm X} - 43.75) + 0.309(1+z)^{0.38}, \quad (12)$$

and noted as 'f2_4', 'f2_5', and 'f2_6', respectively (shown in Fig. 2). Due to the simple linear dependence on luminosity, the type-2 AGN fraction will quickly become zero as luminosity increasing. According to recent results of Brusa et al. (2010), the fraction of the obscured AGN population at the highest ($L_{\rm X} > 10^{44}$erg s^{-1}) X-ray luminosity is $\sim 15\% - 30\%$. So, we have set a lower limit of 0.15 for the evolution of $f_2(\log L_{\rm X}, z)$ to stand for a flattening

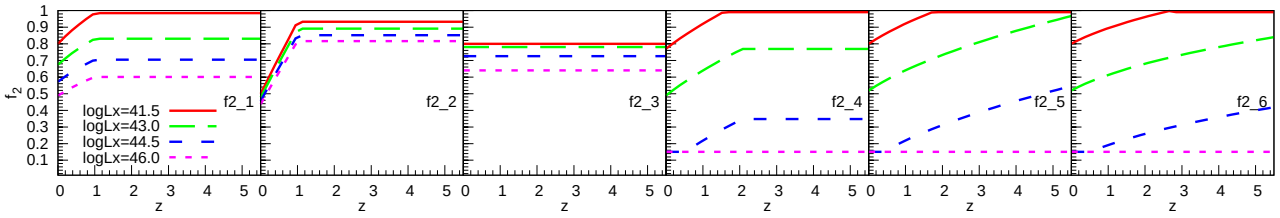

Figure 2. The six evolution models of $f_2(\log L_{\rm X}, z)$ used in this paper are shown at $\log L_{\rm X}$=41.5 (red solid line), 43.0 (green dashed line), 44.5 (blue short dashed line) and 46.0 (purple dot line), respectively. The first three, which are constrained by CXRB spectrum and X-ray number count as given by Ballantyne et al. (2006a), are noted as 'f2_1', 'f2_2', and 'f2_3', respectively. The last three, which are constructed according to recent measurement of Hasinger (2008), are noted as 'f2_4', 'f2_5', and 'f2_6', respectively.(see text for more detailed explanations for these evolution models.)

of the decline at the highest luminosities as expected. Naturally, an upper limit of 1 is forced at all cases.

Except for $f_2(\log L_{\rm X}, z)$, additional assumptions are needed to determine a specific distribution of $N_{\rm H}$. The exact distribution of $N_{\rm H}$ is unknown except for local bright Seyfert 2s (e.g. Risaliti et al. 1999), but the covering factor is a useful parameter for its theoretical description. Here, we use a simple assumption about the distribution of $N_{\rm H}$ following Ballantyne et al. (2006b). In the 'simple $N_{\rm H}$ distribution', ten values of $N_{\rm H}$ are considered: $\log(N_{\rm H}/{\rm cm}^{-2}) = 20, 20.5, \ldots, 24.0, 24.5$, and a type-1 AGN is assumed to have an equal probability p of being absorbed by columns with $\log N_{\rm H} < 22$. Likewise, a type-2 AGN has an equal chance of being absorbed by columns with $\log N_{\rm H} \geqslant 22$:

$$\log(N_{\rm H}/{\rm cm}^{-2}) = \begin{cases} 20.0, \ldots, 21.5, & p = \frac{1-f_2(\log L_{\rm X}, z)}{4.0} \\ 22.0, \ldots, 24.5, & p = \frac{f_2(\log L_{\rm X}, z)}{6.0} \end{cases} \quad (13)$$

Since $f_2(\log L_{\rm X}, z)$ depends on $\log L_{\rm X}$ and z, the distribution of obscuring medium around AGN evolves with both $\log L_{\rm X}$ and z. It is worth noting that this simple assumption about the distribution obscuring medium with different $N_{\rm H}$ is only used to construct $N_{\rm H}$-averaged SEDs (described in the next Section). We do not expect it to give a correct fraction of Compton-thick AGN. In fact, there are AGN with estimated column $\log N_{\rm H} \geqslant 25$ (e.g. NGC 1068; Matt et al. 1997). The inclusion of very Compton-thick obscuring medium dramatically increase the computation time of SEDs. However, they have important effects mainly in the far-IR, but only ignorable effects in the mid-IR which we are mostly interested in currently.

3 MODELLING THE SPECTRAL ENERGY DISTRIBUTION OF AGN

To predict the IR properties of AGN, we must know the relation between IR and X-ray luminosity of AGN. This can be given by the SEDs of AGN with different X-ray luminosities. The SEDs of AGN can be obtained from observations or theoretical calculations. The observational SEDs have the advantage of being based on observations of real AGN. However, the number of observed objects is limited, and they only cover a narrow range of luminosity, redshift and wavelength. Alternatively, we can use theoretical dusty torus emission models, which include a detailed radiative transfer calculation, to compute the expected IR SED for a given X-ray luminosity. However, most radiative transfer calculation for IR dust emission of AGN do not include detailed considerations of gas and its interaction with dust (e.g. Treister et al. 2004, 2006; Nenkova et al. 2008a,b). The gas and dust are expected to be interacting with each other, and gas is responsible for the absorption of X-ray. So, for a reasonable connection of the X-ray and IR properties of AGN, gas and their interaction with dust must be considered.

Here, the calculation of AGN SEDs is performed by using the photoionization code CLOUDY v. 07.02.01 (Ferland et al. 1998), following a procedure similar to that of Ballantyne et al. (2006b), but with some simplifications. In CLOUDY, the atomic gas physics along with the detailed dust radiation physics, such as polycyclic aromatic hydrocarbon (PAH) emission and emission from very small grains, have been self-consistently considered. In addition, many important physical properties of the obscuring medium around AGN, such as its distance from the central engine, gas density, distribution and gas/dust ratio, can be varied freely, and so explored extensively. CLOUDY is a one-dimensional radiative transfer code, and the methods we employed to model the SEDs of AGN are less sophisticated than those used by Treister et al. (2006) or Nenkova et al. (2008a). However, Ballantyne et al. (2006b) showed that the SEDs, when averaged over a $N_{\rm H}$ distribution, have very similar properties to the ensemble of AGN found in the deep surveys of *Chandra*, *XMM-Newton* and *Spitzer*.

3.1 Construction of CLOUDY model

To construct a CLOUDY model, three ingredients must be specified. Firstly, the shape and intensity of the radiation source, which define the incident continuum, must be set. The intrinsic spectrum of AGN is described by a multi-component continuum typical for AGN, which extend from 100 keV to > 1000 μm. Specifically, the 'Big Bump' component, peaking at 1 Ryd, is a rising power law with a high-energy exponential cutoff and parameterized by the temperature of the bump. The big blue bump temperature is set to be a typical value of 10^5K. The X-ray to UV ratio $\alpha_{\rm ox}$, which is defined by

$$\alpha_{\rm ox} = \frac{\log(L_{2\,{\rm keV}}/L_{2500\text{Å}})}{\log(\nu_{2\,{\rm keV}}/\nu_{2500\text{Å}})} = 0.3838\,\log\left(\frac{L_{2\,{\rm keV}}}{L_{2500\text{Å}}}\right), \quad (14)$$

have an important effect on the resulting X-ray to IR ratio. Especially, there are evidences (e.g. Steffen et al. 2006; Hopkins et al. 2007; Vagnetti et al. 2010) that this parameter may be anticorrelated with the UV luminosity of AGN. To explore the effects of this important parameter, we set $\alpha_{\rm ox}$ to be a constant value of -1.5, -1.4 and -1.3, respectively. We also tested the $\alpha_{\rm ox} - L_{\rm UV}$ relation presented in Hopkins et al. (2007), which is given by

$$\alpha_{\rm ox} = -0.107\,\log(\frac{L_{2500\text{Å}}}{{\rm erg\,s^{-1}\,Hz^{-1}}}) + 1.739, \quad (15)$$

and determined specifically for unobscured (type-1) quasars. This results in a luminosity-dependent shape of the input SED from AGN center. The low-energy slope of the Big Bump continuum $\alpha_{\rm uv}$ is set to be the default value of -0.5. The X-ray photon index is assumed to be $\Gamma = 1.9$, and so the energy index $\alpha_{\rm x} = 1 - \Gamma = -0.9$. The full continuum is the sum of two components as given by

$$f_\nu = \nu^{\alpha_{\rm uv}} \exp(-h\nu/KT_{\rm BB}) \exp(-KT_{\rm IR}/h\nu) + a\nu^{\alpha_{\rm x}}, \quad (16)$$

where $T_{\rm BB}$ is the temperature of Big Bump and the coefficient a is adjusted to produce the correct $\alpha_{\rm ox}$ for the case where the Big Bump does not contribute to the emission at 2 keV. The Big Bump component is assumed to have an IR exponential cutoff at $KT_{\rm IR} = 0.01{\rm Ryd}$ (1Ryd $\sim$ 13.6 eV).[1] Finally, this spectrum is scaled to have a luminosity of $L_{2500\text{Å}}({\rm erg\ s^{-1}\ Hz^{-1}})$.

The second ingredient of a CLOUDY model is the chemical composition of the obscuring medium. A gaseous element abundance similar to that of Orion Nebula is assumed. The size distributions and abundances of graphitic, silicate and PAHs grains are also set to be similar to that of Orion Nebula. The obscuring medium is assumed to distribute uniformly and have a constant hydrogen density $n_{\rm H}$ of $10^4{\rm cm^{-3}}$.

The last ingredient of a CLOUDY model is the geometry of the obscuring medium. Here, the obscuring medium is assumed to be $R_{\rm in}$ pc away from the center and with a column density of $N_{\rm H}$. On the other hand, to be consistent with the unified model, Ballantyne et al. (2006b) have set the covering factor of the obscuring medium to f_2 when $N_{\rm H} \geqslant 10^{22}$ cm^{-2} or $1 - f_2$ otherwise, in CLOUDY model. Since f_2 depends on both luminosity and redshift, the CLOUDY simulation needs to be done for each luminosity and redshift, respectively. This would result in a great number of CLOUDY models. However, in CLOUDY models the covering factor only has second-order effects on the spectrum through changes in the transport of the diffuse emission. So, we just use the default geometric covering factor of unity (the shell fully covers the continuum source) but a radiative covering factor of zero, i.e. an open geometry is assumed, and the reflected radiation can be obtained as well. The effects of covering factor on the diffuse and reflected emissions are considered after the CLOUDY simulation as described int the next section.

3.2 CLOUDY model grids and construction of AGN SEDs

The CLOUDY models are built for $L_{2500\text{Å}}({\rm erg\ s^{-1}\ Hz^{-1}})$ [2] from 27 to 34 (in steps of 0.25), and $\log(N_{\rm H}/{\rm cm^{-2}})$ from 20.0 to 24 (in steps of 0.5). Following Ballantyne et al. (2006b), we firstly set $R_{\rm in}$ to be 10 pc. However, we found that the temperatures of grains will be much higher than their sublimation temperatures at the high-luminosity end if a constant $R_{\rm in}$ of 10 pc is assumed. We have practically found a luminosity-dependent $R_{\rm in}$, which is given by

$$R_{\rm in} = 10 * [\frac{\nu L_\nu(2500\text{Å})}{10^{46}}]^{1/2} {\rm pc}, \quad (17)$$

to fix this problem. The CLOUDY models are also built by assuming luminosity-dependent $R_{\rm in}$ for comparison. Finally, as mentioned above, the CLOUDY models are built for four choices of $\alpha_{\rm ox}$, respectively.

[1] See CLOUDY document for more detailed explanations for the construction of this AGN spectrum.

[2] To explore the effects of $L_{\rm UV}$-dependent $R_{\rm in}$ and $\alpha_{\rm ox}$ on the resulting SEDs, $L_{2500\text{Å}}$ instead of $L_{\rm X}$ is used to define the luminosity of input SED.

For each CLOUDY model, three kinds of SEDs are predicted: the attenuated incident continuum, diffuse continuum and reflected continuum. The SEDs with different $N_{\rm H}$ correspond to observations from different direction. However, according to the unified model of AGN, obscuring medium with all values of column density $N_{\rm H}$ simultaneously exist around AGN. On the other hand, there are evidences that obscured and unobscured AGN present more similar $L_{\rm MIR}/L_{\rm X}$ ratios (e.g. Alonso-Herrero et al. 2001; Krabbe et al. 2001; Lutz et al. 2004; Horst et al. 2006, 2008) than that predicted by traditional torus models assuming a smooth distribution of dusty obscuring medium. Recent works (Nenkova et al. 2008a,b; Hönig et al. 2010; Hönig & Kishimoto 2010) show that the distribution of dusty obscuring medium is clumpy rather than contiguous. So, when we observe an AGN from one direction, both diffuse and reflected emission from all $N_{\rm H}$ can be observed, in addition to the attenuated incident emission through an obscuring medium with a column density $N_{\rm H}$ of this direction. For this reason, we have made a modification to the original torus emission model of Ballantyne et al. (2006b). The SED of an AGN with column density $N_{\rm H}$ is constructed by adding the diffuse and reflected emission averaged over all 10 models with different $N_{\rm H}$ to the attenuated incident emission through a particular $N_{\rm H}$. The weights are given by the probability distribution of the column densities, which is a function of $f_2(\log L_{\rm X}, z)$ (or covering factor) as discussed in Section 2.2. The SEDs constructed this way is called 'unified SEDs'.

Finally, the 'unified SEDs' undergo an average over $N_{\rm H}$ again to produce the '$N_{\rm H}$-averaged SEDs', which will be used to predict the IRLFs of AGN later. Here, three types of $N_{\rm H}$-averaged SEDs are constructed. The type-1 SED is an average of the 'unified SEDs' with $10^{20.0}{\rm cm^{-2}} \leqslant {\rm N_H} < 10^{22}{\rm cm^{-2}}$. The type-2 SED is an average of the 'unified SEDs' with $10^{22}{\rm cm^{-2}} \leqslant {\rm N_H} \leqslant 10^{24.5}{\rm cm^{-2}}$. The average SED is an average of the 'unified SEDs' with $10^{20.0}{\rm cm^{-2}} \leqslant {\rm N_H} \leqslant 10^{24.5}{\rm cm^{-2}}$. As an example, Fig 3 shows the rest-frame SEDs taken from the 'f2_1' evolutionary grid (eq. 7) for a Seyfert-like AGN ($L_{\rm X} = 10^{43.54}{\rm erg\ s^{-1}}, z = 0.7, f_2 = 0.7484$) and quasar-like AGN ($L_{\rm X} = 10^{46.54}{\rm erg\ s^{-1}}, z = 1.4, f_2 = 0.5705$), respectively.

3.3 Testing model SEDs of AGN

The method we have used to model the SEDs of AGN is similar to that of Ballantyne et al. (2006b). They have been extensively tested this method against large samples of AGNs. Here, we present two additional tests that are more directly related to the goal of this paper, i.e. prediction of IRLFs from HXLF. For this goal, the most important thing is correct X-ray to IR relation.

Recently, Gandhi et al. (2009) found a strong mid-infrared:X-ray ($\log\lambda L_\lambda(12.3\mu{\rm m})$-$\log L_{2-10{\rm keV}}$) luminosity correlation for a sample of local Seyferts, the cores of which have been resolved in the mid-IR. The relation is given by

$$\log\lambda L_\lambda(12.3\mu{\rm m}) = -4.37 + 1.106\log L_{2-10{\rm keV}}, \quad (18)$$

and is found to be valid in a wide range of luminosity and may extend into the quasar regime. Mullaney et al. (2011) converted this correlation to that between $\log L_{\rm IR}$ and $\log L_{2-10{\rm keV}}$, which is given by

$$\log\frac{L_{\rm IR}}{10^{43}{\rm erg\ s^{-1}}} = 0.53 + 1.11\log\frac{L_{2-10{\rm keV}}}{10^{43}{\rm erg\ s^{-1}}}. \quad (19)$$

In Fig 4, the $\log L_{\rm IR}$-$\log L_{2-10{\rm keV}}$ relation computed from our model SEDs of AGN by using different choices of $\alpha_{\rm ox}$

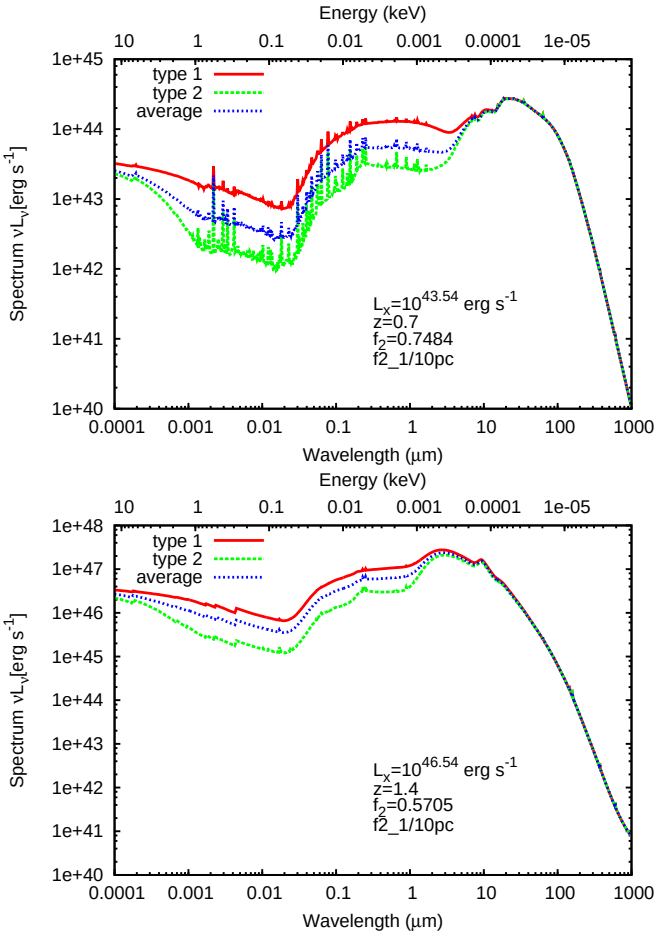

Figure 3. Top: Rest-frame SEDs for a Seyfert-like AGN ($L_{\rm X} = 10^{43.5}{\rm erg\ s^{-1}}$) at $z = 0.7$ and obscured by dusty medium with an inner radius 10 pc, hydrogen density $n_{\rm H} = 10^4{\rm cm^{-3}}$ and covering factor $f_2 = 0.7484$. The type-1 SED is shown in red, the type-2 SED is shown in green, while the average SED is shown in blue. Bottom: As top, but for a quasar-like AGN ($L_{\rm X} = 10^{46.5}{\rm erg\ s^{-1}}$) at $z = 1.4$ and obscured by dusty medium with a covering factor $f_2 = 0.5705$. These spectrums are taken from the 'f2_1' evolutionary grid (eq. 7).

and $R_{\rm in}$ are tested against the observational relation given by Mullaney et al. (2011). As shown in the figure, the result obtained for $\alpha_{\rm ox} = -1.4$ and $R_{\rm in} = 10$ pc (as in Ballantyne et al. (2006b)) significantly deviates from the nearly linear relation given by Mullaney et al. (2011). This problem has also been noticed by Draper & Ballantyne (2011). We found that a more linear $\log L_{\rm IR}$-$\log L_{2-10{\rm keV}}$ relation can be obtained if $R_{\rm in}$ decreases with $L_{\rm UV}$ (as given by Eq. 17). With the typical value of $\alpha_{\rm ox} = -1.4$, this lead to a result similar to that of Mullaney et al. (2011), especially at the high-luminosity range. At the low-luminosity range, a larger $\alpha_{\rm ox}$ seems required. However, when the $\alpha_{\rm ox}$-$L_{\rm UV}$ relation given by Hopkins et al. (2007) (as given by Eq. 15) is assumed, a too steep relation is obtained. So, these results support the anticorrelation between $\alpha_{\rm ox}$ and $L_{\rm UV}$ found by other independent observations (e.g. Steffen et al. 2006; Vagnetti et al. 2010), but imply a more flat relation.

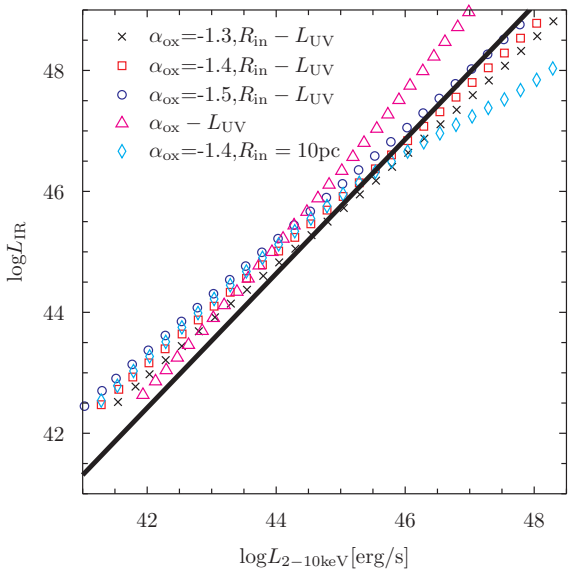

Figure 4. Test of the $\log L_{\rm IR}$-$\log L_{2-10{\rm keV}}$ relation computed from our model SEDs of AGN against the observational relation (black-solid line) given by Mullaney et al. (2011). The results obtained by using different choices of $\alpha_{\rm ox}$ and $R_{\rm in}$ are presented, respectively. The $L_{\rm UV}$-dependent $R_{\rm in}$ is given by Eq. 17, while the $L_{\rm UV}$-dependent $\alpha_{\rm ox}$ is given by Eq. 15.

4 CONNECTING X-RAY AND IR

The IR is less affected by the selection effects due to obscuration suffered by optical and X-ray, while X-ray is currently the most efficient for selecting AGN to high redshifts. Connecting X-ray and IR can provide a more clear view on the evolution of AGN populations. If the evolution of AGN shown in HXLF and f_2, which are revealed mainly from X-ray observations, are intrinsic, they should be shown somehow in the directly observed IRLFs of AGN.

4.1 The mid-IR LFs of type-1 and/or type-2 AGN

Since the HXLF tells us how the number density of AGN per increment of $\log L_{\rm X}$ changes with z and $L_{\rm X}$, the following expression can be used to relate HXLF to IRLFs ${\rm d}\Phi/{\rm d}(\log\nu L_\nu)$:

$$\frac{{\rm d}\Phi}{{\rm d}(\log\nu L_\nu)} = \frac{{\rm d}\Phi}{{\rm d}(\log L_{\rm X})}\frac{{\rm d}(\log L_{\rm X})}{{\rm d}(\log\nu L_\nu)}. \qquad (20)$$

Here, ${\rm d}\Phi/{\rm d}(\log L_{\rm X})$ is the HXLF of AGN given in Section 2.1, and L_ν is the luminosity at a given wavelength.

In Section 3, we have obtained the SEDs spanning from X-ray all the way to IR for AGN with different luminosities and redshifts. So, the dependence of IR luminosity on hard X-ray luminosity, as described by ${\rm d}(\log L_{\rm X})/{\rm d}(\log\nu L_\nu)$, can be obtained from the SEDs easily. For predicting the IRLFs for total AGN (type-1 + type-2), we use the average SED presented in Section 3. The IRLF of AGN is not an integrated quantity, and so much more sensitive to the evolution trends in the HXLF and the f_2 than the cumulative number count distribution and background spectra intensity of AGN. Using the IRLFs for total AGN has the advantage of being independent of the methods used to do a further classification of AGN, such as detailed optical emission line spectra, or an accurate measurement of X-ray absorbing column densities $N_{\rm H}$. For these reasons, Ballantyne et al. (2006b) suggested to use IRLFs for total AGN to distinguish different evolution models of AGN obscuration. However, the results of Ballantyne et al. (2006b) showed that

the IRLFs is not very sensitive to the evolution model of AGN obscuration unless at much longer IR wavelengths where the contaminant from star formation is important.

The separated IRLFs for type-1 and type-2 AGN respectively are expected to be much more sensitive to the overall evolution of AGN spatial density and obscuration, although a detailed classification are required. The classification of AGN into type-1 and type-2 involves with the problem of consistency between different classification methods. However, this may be a possible key to the problem of the evolution of AGN obscuration, since inconsistent classification methods will directly result in very different conclusions for the evolution of AGN obscuration. By separating the IRLFs to that for type-1 and type-2 AGN, the intrinsic evolution of AGN and the variations just resulted from the evolution of AGN obscuration, can be investigated in more detail and possibly clarified. Furthermore, by considering the IRLFs for type-1 and type-2 AGN separately, the modeling of AGN SEDs can be further constrained. So, it would be more fruitful to separate the IRLFs of AGN into that for type-1 and type-2, respectively. This may provide a more useful tool to explore the properties of obscuring medium around different types of AGN.

The separated IRLFs of type-1 and type-2 AGN are given as,

$$\frac{\mathrm{d}\Phi_1}{\mathrm{d}(\log\nu L_\nu)} = \frac{\mathrm{d}\Phi}{\mathrm{d}(\log L_{\rm X})}(1 - f_2(\log L_{\rm X}, z))\frac{\mathrm{d}(\log L_{\rm X})}{\mathrm{d}(\log\nu L_\nu)}, \quad (21)$$

and

$$\frac{\mathrm{d}\Phi_2}{\mathrm{d}(\log\nu L_\nu)} = \frac{\mathrm{d}\Phi}{\mathrm{d}(\log L_{\rm X})} f_2(\log L_{\rm X}, z)\frac{\mathrm{d}(\log L_{\rm X})}{\mathrm{d}(\log\nu L_\nu)}, \quad (22)$$

where $f_2(\log L_{\rm X}, z)$ is the fraction of type-2 AGN. We use the type-1 SED presented in Section 3 to predict the IRLFs of type-1 AGN, while using the type-2 SED to predict the IRLFs of type-2 AGN.

5 RESULTS

In this section, we present the predicted mid-IR LFs for total, type-1 and type-2 AGN, respectively. The SEDs of AGN used to obtain the X-ray to IR luminosity relation are computed by assuming a constant $\alpha_{\rm ox} = -1.4$, and $L_{\rm UV}$-dependent $R_{\rm in}$ as described by Eq. 17. We leave the discussion of $L_{\rm UV}$-dependent $\alpha_{\rm ox}$ in Section 6. The results for all combinations of HXLF as given in Section 2.1 and different evolution models of AGN obscuration as given in Section 2.2 are presented and then compared with the measurements of mid-IR LFs of AGN currently available, respectively. Since we are mainly interested in finding out much obvious trends, a simple qualitative comparison by eye rather than a much detailed fitting [3], is taken here.

5.1 The mid-IR LFs of total AGN

In Figs. 5 and 6, the predicted rest-frame 8.0 and 15 μm LF for total AGN are shown. In each panel, the results are predicted from an evolution model of HXLF and six evolution models of AGN obscuration as discussed in Section 2.2. The observational results used for comparison are from Fu et al. (2010). They used high-quality *Spitzer* $7-38$ μm spectra to cleanly separate star formation and AGN in individual galaxies for a 24 μm flux-limited sample of galaxies at $z\sim0.7$, and decomposed the mid-IR LFs between star formation and AGN.

[3] Much more careful considerations of the covariance between points or systemic errors are not included as well.

As can be clearly seen in Figs. 5 and 6, our results agree with that of Fu et al. (2010), Matute et al. (2006) and Hopkins et al. (2007) reasonably. These general agreements show that the methods we have used to model the SEDs of AGN and to predict corresponding mid-IR LFs from HXLF are basically reasonable. Specifically, different evolution models of HXLF give very similar results at $8.0\ \mu$m and $15\ \mu$m. However, different evolution models of AGN obscuration are distinguishable at $15\ \mu$m, while not at $8.0\ \mu$m. As shown in Fig 6, the results at $15\ \mu$m are divided into two groups, corresponding to using models from Ballantyne et al. (2006a) and using models constructed according to recent results of Hasinger (2008), respectively. The results predicted by using the evolution models of AGN obscuration from Ballantyne et al. (2006a) are in a better agreement with the measurements of Fu et al. (2010) and the results from other authors, especially at the relative higher luminosities. It seems that the evolution of AGN obscuration are better described by the models of Ballantyne et al. (2006a) at the redshift and luminosity ranges covered by the measurements of Fu et al. (2010), i.e. $z\lesssim1$ and $\nu L_\nu(8.0\ \mu{\rm m}, 15\ \mu{\rm m}) < 10^{12}{\rm L}_\odot$.

5.2 The mid-IR LFs of type-1 AGN and type-2 AGN

As mentioned above, it is more fruitful to separate the mid-IR LFs to that for type-1 and type-2 AGN, respectively. Here, we present the mid-IR LFs for type-1 and type-2 AGN and then compare them with the mid-IR observational results of Brown et al. (2006) and Matute et al. (2006), respectively.

5.2.1 The 8.0 μm *LF of type-1 AGN*

From a sample consisting of 292 24 μm sources brighter than 1 mJy selected from *Spitzer* MIPS survey, Brown et al. (2006) have determined the rest-frame 8.0 μm LF for type-1 quasars with $1<z<5$ and $1.5<z<2.5$, respectively. Ballantyne et al. (2006b) used these results (in their Fig. 13), but compared them with the predicted mid-IR LFs for total AGN. Despite this, they found that the predicted and measured LFs show a surprising agreement. As suggested by Brown et al. (2006), if the fraction of obscured quasars decreases rapidly with increasing luminosity, the type-1 quasar LF given by them would appropriate the LF of all quasars at the highest luminosities. However, if there are indeed very few type-2 AGN at very high luminosities, and the type-1 AGN LF provide good approximation of the total LF at the high luminosities, then this would be an important constraint for the evolution of AGN obscuration at high luminosities. This important information was not fully utilized in the method of Ballantyne et al. (2006b). So, it would be more reasonable and fruitful to predict the mid-IR LFs for only type-1 AGN from different evolution models of HXLF and obscuration of AGN, and then compare them with the measurements of Brown et al. (2006).

In Fig. 7, we present the predicted rest-frame 8.0 μm LF of type-1 AGN at $z=1.5, 2.0$, and 2.5, and compare them with the measurements of Brown et al. (2006). As expected, the results predicted from different evolution models of AGN obscuration are more distinguishable when the rest-frame 8.0 μm LF for only type-1 AGN, instead of total AGN, are used. The rest-frame 8.0 μm LF of type-1 AGN predicted from different choices of HXLF tend to underestimate the number of AGN as measured by Brown et al. (2006), and no matter which evolution model of AGN obscuration is used. Surprisingly, using the HXLF of Ueda et al. (2003) result in a better agreement with the measurements of Brown et al. (2006)

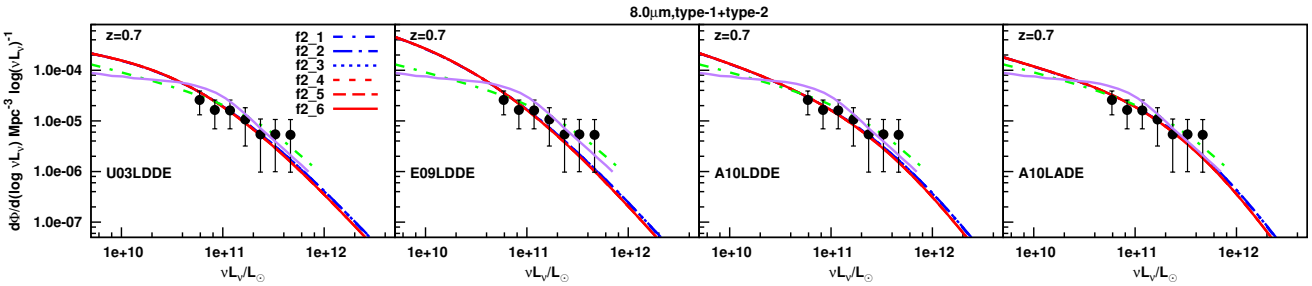

Figure 5. Rest-frame 8.0 μm LF for total AGN at $z = 0.7$ as predicted from the LDDE modeling of HXLF of Ueda et al. (2003), Ebrero et al. (2009), Aird et al. (2010), and the LADE modeling of HXLF of Aird et al. (2010), respectively. At each panel, the results for six evolution models of f_2 are presented. The blue lines show the results for the three evolution models of f_2 given by Ballantyne et al. (2006a), who constrained the evolution of f_2 by fitting to the shape of CXRB spectrum and X-ray number counts. The short dashed-doted, long dashed-doted, and doted lines show the results for the 'f2_1', 'f2_2', and 'f2_3' evolution models, respectively. The red lines show the results for the three evolution models of f_2 given by Hasinger (2008) from direct X-ray observations of the evolution of type-2 AGN fraction. Here, the short-dashed, long-dashed, and solid lines show the results for the 'f2_4', 'f2_5', and 'f2_6' evolution models, respectively. The data points are the 8.0 μm IRS-decomposed AGN LF of Fu et al. (2010) at $z \sim 0.7$. The green dot-dashed lines show the obscuration-corrected AGN bolometric LF of Hopkins et al. (2007) (taken from Fu et al. (2010)). The purple solid lines show the LF for total AGN of Matute et al. (2006) as combined and converted to 8.0 μm at $z \sim 0.7$ by Fu et al. (2010).

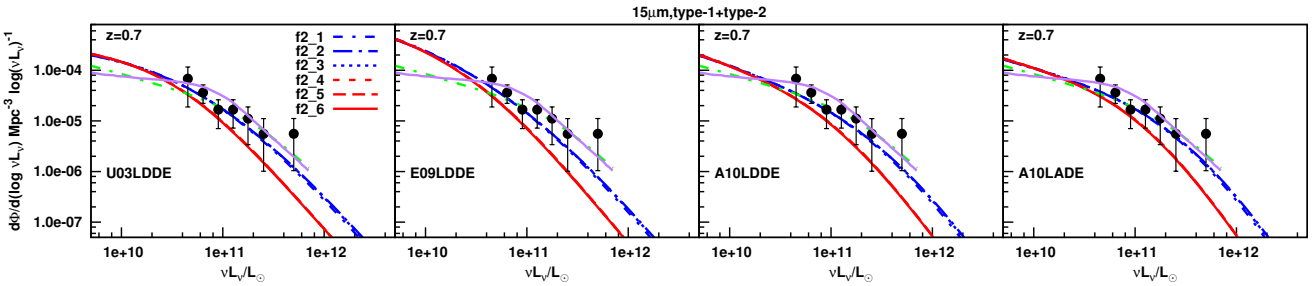

Figure 6. Similar to Fig. 5, but for the 15 μm LF. The AGN obscuration evolution models of Ballantyne et al. (2006b) give better agreements with the measurements of Fu et al. (2010), Matute et al. (2006), and the results of Hopkins et al. (2007).

than using all the more recent HXLF measurements. The results shown here may have, to some extent, confirmed the credibility of widely used results of Ueda et al. (2003). However, this may just be a coincidence, since more recent observational determination of HXLF are generally expected to be more accurate. More reasonable conclusions can only be obtained from comparisons with other independent measurements.

5.2.2 The 15 μm LF of type-1/type-2 AGN

From a sample of AGN selected at 15 μm (ISO) and 12 μm (IRAS), Matute et al. (2006) measured the rest-frame 15 μm LF of type-1 and type-2 AGN, which are classified based on their optical spectra, separately. In Figs. 8 and 9, we show the predicted rest-frame 15 μm LF for type-1 AGN and type-2 AGN and compare them with the results of Matute et al. (2006).

Fig. 8 presents the rest-frame 15 μm LF of type-1 AGN at $z = 0.1$ and 1.2. As can be clearly seen, the predicted results show reasonable agreements with the measurements of Matute et al. (2006). However, it is also clear, especially at $z = 1.2$, that the predicted IRLFs tend to underestimate the number of the most IR-luminous type-1 AGN, which is independent of the choices of the evolution of HXLF and obscuration. Interestingly, the measurements at $z = 0.1$ can be basically explained by the results predicted from most HXLFs. The only exception is the result predicted from the HXLF of Aird et al. (2010) modeled with LADE, which significantly underestimated the number of the most IR-Luminous AGN even at $z = 0.1$. Similar to that shown in Fig. 7, these results show that the mid-IR LFs predicted from HXLF tend to underestimated the number of the most IR-luminous AGN, and become significant at $z \gtrsim 1$.

Fig. 9 presents the rest-frame 15 μm LF of type-2 AGN at $z = 0.05$ and 0.35. As mentioned by Matute et al. (2006), the observational determination of the rest-frame 15 μm LF of type-2 AGN is much poorer than that of type-1 AGN. So, their measurement of the density of type-2 AGN can only be considered as a lower limit. However, as can be seen in Fig. 9, the results predicted from the AGN obscuration evolution models that are constructed according to the results of Hasinger (2008) tend to underestimate even the number of type-2 AGN currently measured. Due to the much bigger uncertainties in the measurements of the 15 μm LF of type-2 AGN, more definitive conclusions cannot be drawn.

6 DISCUSSION

By separating the mid-IR LFs of AGN to that for type-1 and type-2 AGN respectively, the modeling of AGN SEDs, the evolution of LFs and obscuration of AGN can be further constrained. The results presented in the Section 5 show that the mid-IR LFs predicted from HXLF tend to underestimate the number of the most IR-luminous AGN, despite of the general agreements between predictions and measurements. This is independent of the choices of the evolution models of HXLF and obscuration of AGN, and even more obvious

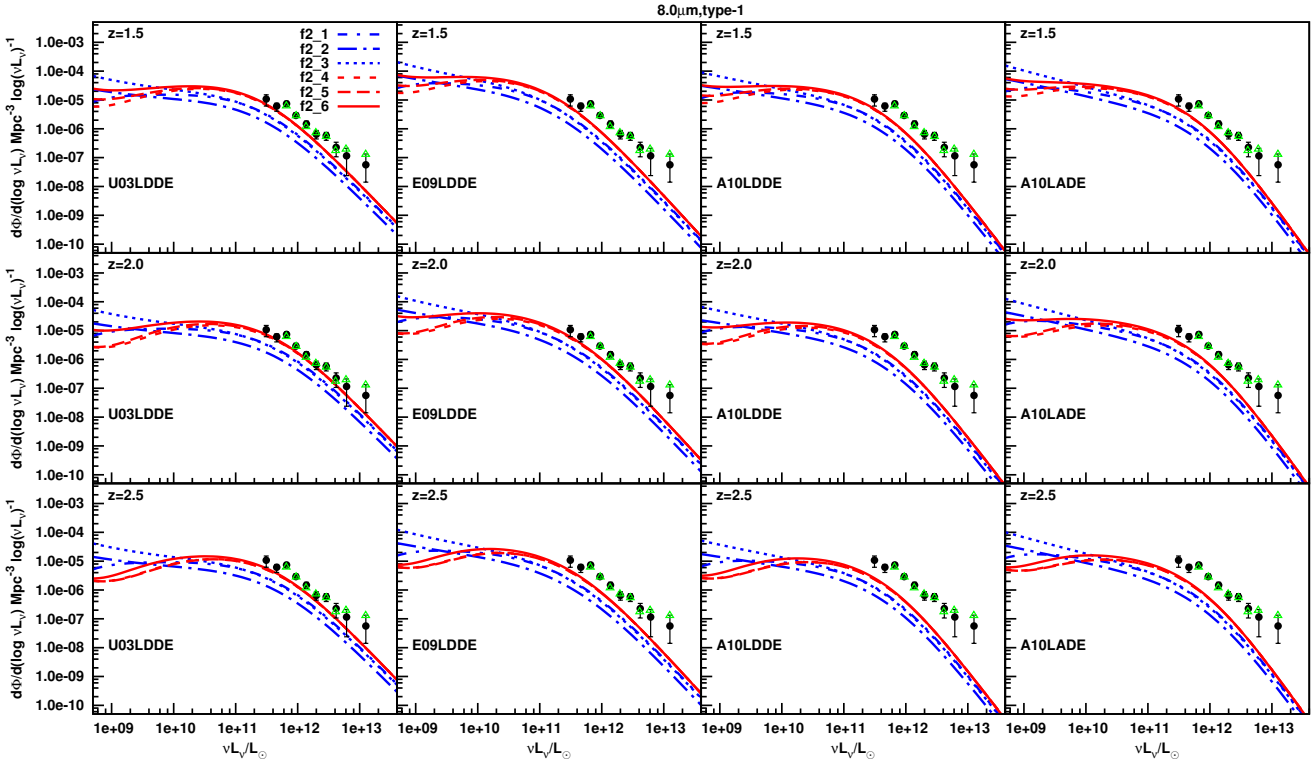

Figure 7. Rest-frame 8.0 μm LF for type-1 AGN at $z = 1.5, 2.0$, and 2.5 as predicted from the LDDE modeling of HXLF of Ueda et al. (2003), Ebrero et al. (2009), Aird et al. (2010), and the LADE modeling of HXLF of Aird et al. (2010), respectively. At each panel, the results for six evolution models of f_2 are presented with line styles and colours that are the same as in Fig. 5. The data points show the measured 8.0 μm LF of type-1 quasars as determined by Brown et al. (2006) from a sample consists of 292 24 μm sources brighter than 1 mJy and selected from *Spitzer* MIPS survey. The black solid points denote the result for objects over the redshift range $1 < z < 5$, and the green triangles for those with $1.5 < z < 2.5$. All the results predicted from HXLF, especially those recently presented, tend to underestimate the number of IR-luminous AGN, independent of the choices of the evolution of HXLF and obscuration.

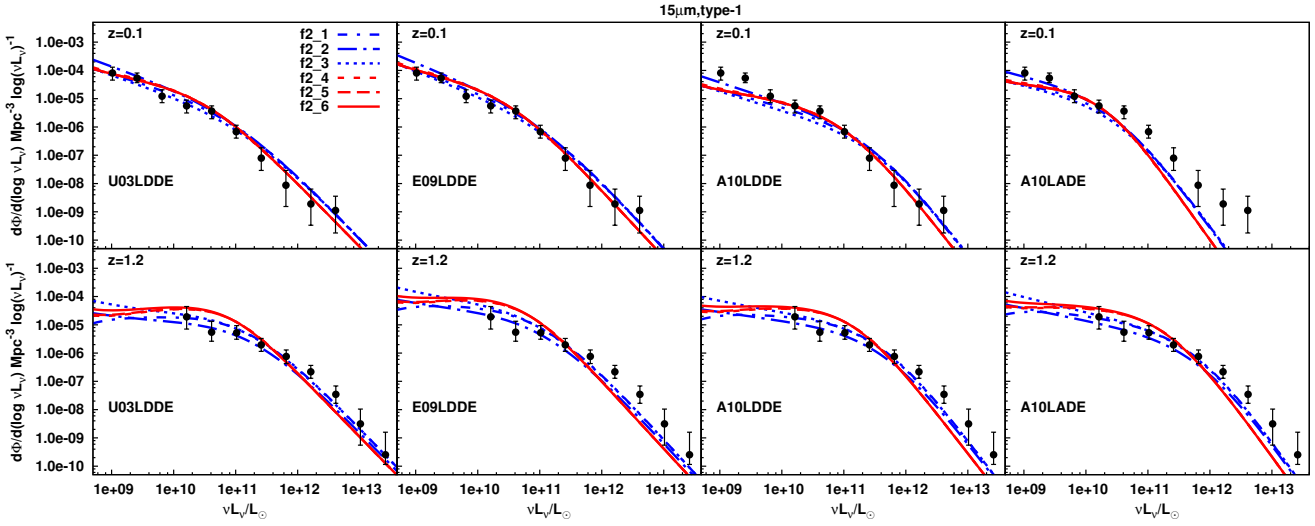

Figure 8. Rest-frame 15 μm LF for type-1 AGN at $z = 0.1$, and 1.2 as predicted from the LDDE modeling of HXLF of Ueda et al. (2003), Ebrero et al. (2009), Aird et al. (2010), and the LADE modeling of HXLF of Aird et al. (2010), respectively. The data points are the measured 15 μm LF of type-1 AGN determined by Matute et al. (2006) from a sample of type-1 AGN with redshift in $z = [0, 0.2]$ (top) and $z = [0.2, 2.2]$ (bottom) selected at 15 μm (ISO) and 12 μm (IRAS), and classified by their optical spectra. At each panel, the results for six evolution models of f_2 are presented with line styles and colours as in Fig. 5. The results predicted from all HXLFs tend to underestimate the number of the most IR-luminous AGN at $z = 1.2$. However, this is not the case at $z = 0.1$, unless the LADE modeling of HXLF of Aird et al. (2010) is used.

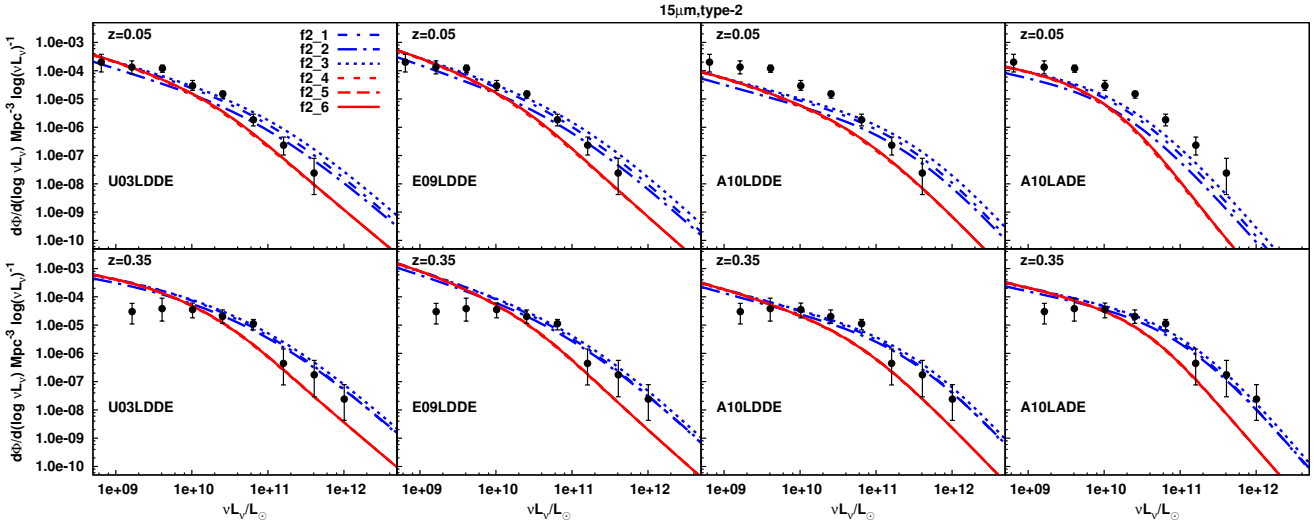

Figure 9. Similar to Fig. 8, but for type-2 AGN at $z = 0.05$, and 0.35. The data points are the measured 15 μm LF of type-2 AGN determined by Matute et al. (2006) from a sample of type-2 AGN with redshift in $z = [0, 0.1]$ (top) and $z = [0.1, 0.6]$ (bottom) selected at 15 μm (ISO) and 12 μm (IRAS), and classified by their optical spectra. The measurement of the mid-IR LF of type-2 AGN is much poorer than that of type-1 AGN, and therefore, is much harder to be explained. However, the results predicted from the AGN obscuration evolution model constructed according to the results of Hasinger (2008) are below even the current measurements.

for the HXLFs recently proposed. Meanwhile, this trend seems not significant for AGN with $z \lesssim 1$ and/or less luminous at IR.

Here, we discuss some possible explanations for this contradiction between HXLFs and mid-IR LFs. Firstly, this may be caused by the missing fraction of AGN, especially those heavily obscured Compton-thick AGN that cannot be detected by current X-ray observations. Recently, Fu et al. (2010) compared their mid-infrared spectroscopic selection with other AGN identification methods and concluded that only half of the mid-infrared spectroscopically selected AGN were detected in X-ray. However, after considering this we find that it only result in a slight improvement to the prediction of IRLFs from HXLF. Furthermore, this explanation needs a larger fraction of missing AGN at the high-luminosity end, which is in contradiction with the general expectation that AGN dominate in the most IR-luminous sources.

Secondly, the contribution of star formation in AGN host to mid-IR, which has not been considered yet, may be important. If this is important, the X-ray to mid-IR relation used to predict mid-IR LFs from HXLFs in Section 5 needs to be corrected significantly. This is particularly important for sources that are not spatially resolved, or with intensive star formation near the nuclear region (Lutz et al. 2004; Horst et al. 2008). We find that if the contribution of star formation in the host to 8.0 μm and 15 μm emission are comparable to the reprocessed nuclear emission, the 8.0 μm and 15 μm LF predicted from HXLF can be consistent with corresponding mid-IR measurements. Currently, it is still difficult to separate the contribution of star formation and AGN to the IR emission of galaxies, especially in systems where the two are comparable and their additive effects are non-linear (Hopkins et al. 2010). Especially, the relative fractions of their contributions to mid-IR are likely to be different in different kinds of galaxies, and may change with both luminosity and redshift of the source. However, even for powerfully star-forming quasars, the contribution of star formation to mid-IR is small (Netzer et al. 2007). So, the possible contribution of star formation to mid-IR is not likely the main reason for the contradiction.

Thirdly, the contradiction found in Section 5 may represent limitations in the torus model used so far. Although the simple torus model inherited from Ballantyne et al. (2006b) has been well tested, the distribution and composition of the obscuring medium around AGN are still very uncertain. Meanwhile, this CLOUDY based torus model essentially assume a smooth distribution of dusty obscuring medium. Recently, a clumpy distribution of dusty obscuring medium is suggested by some authors (Nenkova et al. 2002; Hönig et al. 2006). These authors have recently proposed sophisticated clumpy torus models (Nenkova et al. 2008a,b; Hönig et al. 2010; Hönig & Kishimoto 2010) that are in a better agreement with current IR observations of AGN. Unfortunately, these clumpy torus models mainly give the IR emission properties of AGN, while the self-consistent hard X-ray property is not presented. To give the X-ray to mid-IR luminosity ratios that are more comparable to the observational results of Mullaney et al. (2011), we have made some improvements to the original torus model of Ballantyne et al. (2006b). However, the improved torus model still have some limitations, which is worth additional efforts but is beyond the scope of this paper.

Finally, as shown in Section 3.3, the anticorrelation between $\alpha_{\rm ox}$ and $L_{\rm UV}$, which has been found by many observations, is important for giving X-ray to mid-IR luminosity ratios that are more comparable to the result of Mullaney et al. (2011). Here, we present the results obtained by assuming $\alpha_{\rm ox} = -1.5$ instead of the typical value of -1.4 as used in Section 5. As can be seen in Figs. 10 and 11, the mid-IR LFs measurements of Brown et al. (2006) and Matute et al. (2006) can now be explained much better by the results predicted from the HXLFs recently proposed, especially that of Ebrero et al. (2009). On the other hand, it is interesting to notice the dramatical difference between the results in Figs. 10 and 11. The 8.0 μm LF measurement of Brown et al. (2006) is for luminous quasars with $z > 1$, while the 15 μm LF of Matute et al. (2006) is mainly for Seyferts at much lower luminosities and redshifts. While the results at 8.0 μm favor the obscuration evolution models constructed according to the results of Hasinger (2008), the

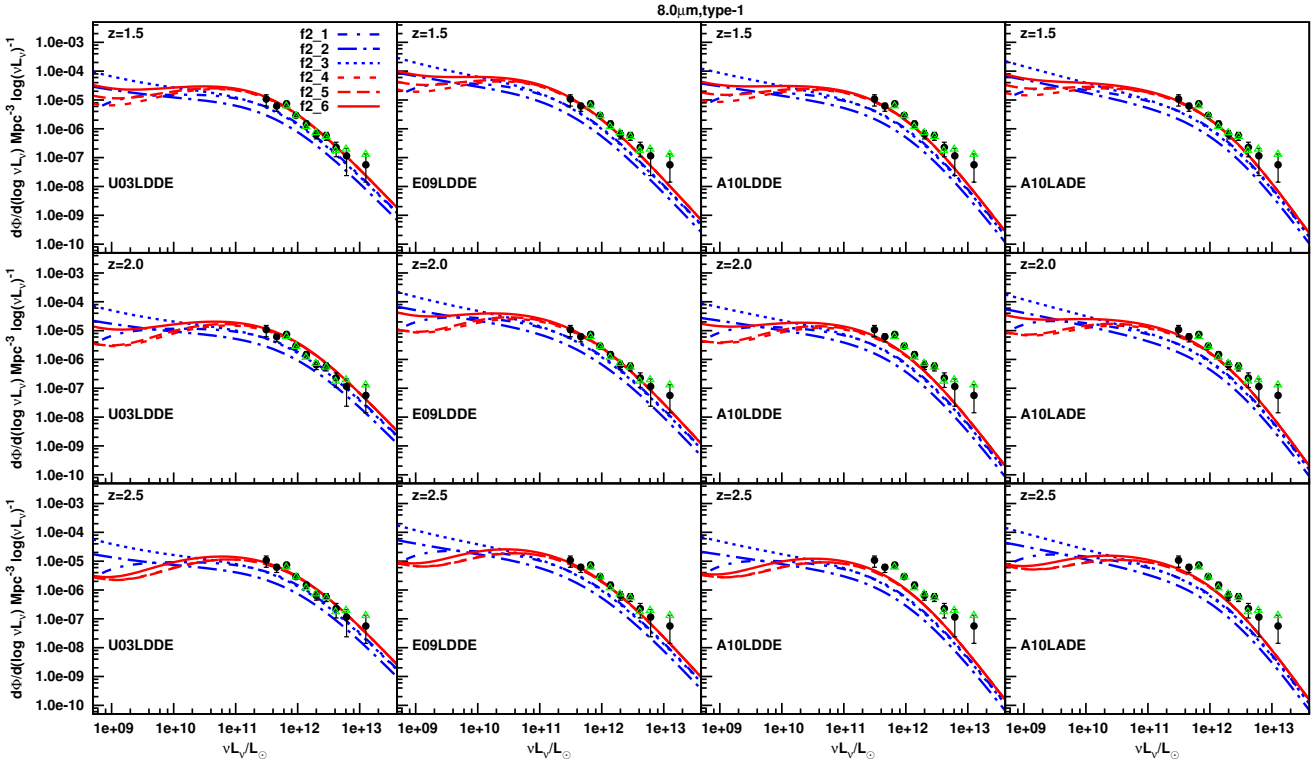

Figure 10. Similar to Fig. 7, but now $\alpha_{\rm ox}$ is assumed to have a smaller value of -1.5 instead of the typical value of -1.4 as used in Section 5. As can be seen, the results have been largely improved after this small change. Now, the measurements of Brown et al. (2006) can be well explained by recently proposed HXLF, especially that of Ebrero et al. (2009), when combined with the obscuration evolution models constructed according to the results of Hasinger (2008). An even smaller $\alpha_{\rm ox}$ seems required at $\nu L_\nu(8.0\ \mu{\rm m}) \gtrsim 5 * 10^{12} {\rm L}_\odot$.

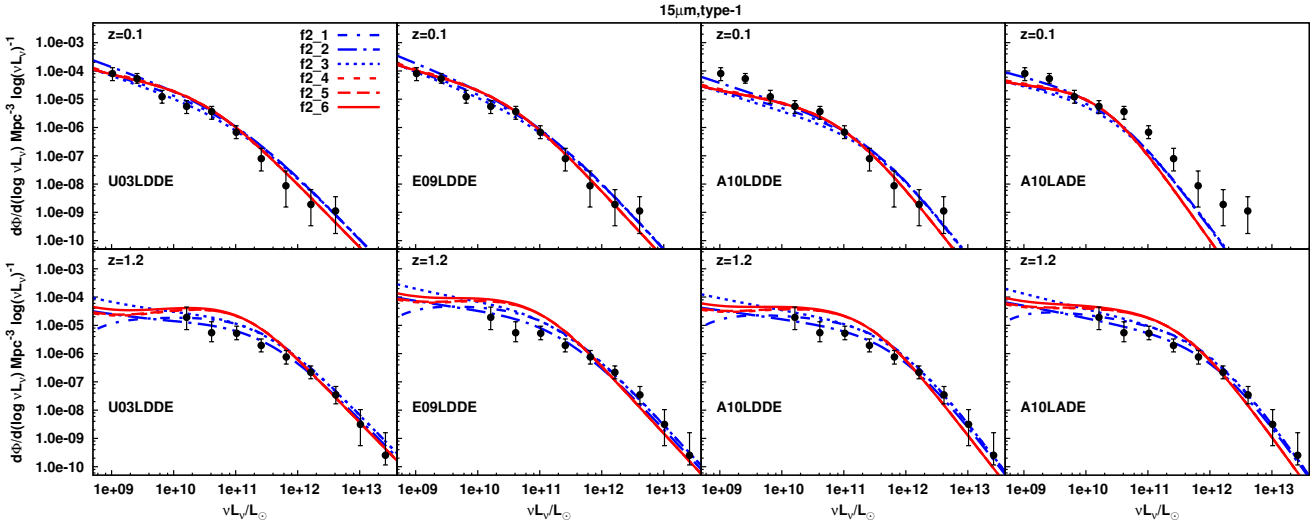

Figure 11. Similar to Fig. 8, but now $\alpha_{\rm ox}$ is assumed to have a smaller value of -1.5 at $z = 1.2$ instead of the typical value of -1.4 as used in Section 5. At $z = 1.2$, it is clear that the results at highest luminosities have been largely improved. Now, the AGN obscuration evolution models proposed by Ballantyne et al. (2006a) seems more favored. However, the change of $\alpha_{\rm ox}$ is not required at $z = 0.1$, unless the LADE modeling of HXLF of Aird et al. (2010) is used.

results at $15\ \mu{\rm m}$ nevertheless give more supports to the models proposed by Ballantyne et al. (2006a).

These results imply that the obscuration of quasars are different from that of Seyferts. Luminous quasars often associate with galaxy major mergers (Canalizo & Stockton 2001) or interactions (Hutchings 1987; Disney et al. 1995; Bahcall et al. 1997; Kirhakos et al. 1999), while there are little observational evidences for less luminous Seyfert galaxies being associated with mergers (Laurikainen & Salo 1995; Schmitt 2001; Grogin et al. 2005). If the evolution and fueling mechanisms of quasars are very differ-

ent from that of lower luminosity Seyfert galaxies, it is natural to expect that the distribution and evolution of the obscuring medium around them are very different. As pointed out by Ballantyne et al. (2006b), the dusty mediums obscuring luminous quasars are likely distributed in a larger scale and linked to the starburst region, while lower luminous quasars and Seyferts are obscured by commonly suggested compact torus located at much smaller scale.

7 SUMMARY

We have presented a detailed comparison between the $2-10$ keV HXLFs and mid-IR LFs of AGN. The combination of hard X-ray and mid-IR provide complementary views for understanding the evolution of LFs and obscuration of AGN and their co-evolution with galaxies. Four measurements of the HXLF of AGN have been collected from the literatures for comparison. A simple but well tested torus model, which is based on photoionization and radiative transfer code CLOUDY, is then employed to model the composite X-ray to IR SEDs for AGN with different luminosities and redshifts. In the modeling of SEDs, we have assumed six evolution models of AGN obscuration, which are constrained by the CXRB (Ballantyne et al. 2006a), or constructed according to recent direct measurement (Hasinger 2008). The model SEDs of AGN have been tested against the observational relations between X-ray and mid-IR luminosity of AGN recently given by Mullaney et al. (2011). The mid-IR LFs predicted from different combinations of the evolution models of HXLF and obscuration of AGN are compared with the measurements of AGN mid-IR LFs given by Brown et al. (2006), Matute et al. (2006), and Fu et al. (2010), respectively. By predicting mid-IR LFs for type-1 AGN, type-2 AGN, and total AGN from HXLF, and comparing them with corresponding observational results respectively, the evolution of LFs and obscuration of AGN can be further understood.

We find that the mid-IR LFs predicted from HXLFs tend to underestimate the number of the most IR-luminous AGN, which is independent of the evolution model of AGN obscuration. We discussed possible explanations for this contradiction. It may partly due to the missing fraction of Compton-thick AGN that have been predicted by the synthesis model of CXRB, but systematically missed by current X-ray observations. However, we find that the underestimation to the number of the most IR-luminous AGN cannot be eliminated even an extreme assumption, which claims that only half of the mid-infrared spectroscopically selected AGN are detected in current X-ray observations, is employed.

We conclude that the contradiction mainly result from limitations in the modeling of the composite X-ray to IR SEDs of AGN. A possible reason is the contribution of star formation in the AGN host to mid-IR, which has not been considered yet. We find that the contribution of star formation to the 8.0 μm and 15 μm emission need to be comparable with that of reprocessed nuclear emission and even more in the most IR-Luminous sources to eliminate the contradiction. However, the contribution of star formation in AGN host to mid-IR is not likely so large but actually decreases with increasing $L_{\rm IR}$. On the other hand, the contradiction may represent limitations in the torus model employed. It is clear that the torus model are further constrained to give the specific prediction of mid-IR LFs for type-1 and type-2 AGN, respectively. We have made some improvements to the original torus model of Ballantyne et al. (2006b), such as a different handling of the diffuse emission and $L_{\rm UV}$-dependent $R_{\rm in}$, to give the X-ray to mid-IR luminosity ratios that are more comparable to the observational results of Mullaney et al. (2011). Meanwhile, with some tests we find that the anticorrelation between $\alpha_{\rm ox}$ and $L_{\rm UV}$ is important for making the X-ray to mid-IR luminosity ratios closer to the results of Mullaney et al. (2011). Interestingly, a smaller $\alpha_{\rm ox}$ improves the prediction of the high-$L_{\rm IR}$ end of the IRLFs significantly at the same time.

Finally, with all the improvements mentioned above, we find that the HXLFs and IRLFs of AGN can be more consistent with each other if the obscuration mechanisms of quasars and Seyferts are assumed to be different. This is consistent with the idea that the obscuration mechanism of luminous quasars dominating at high redshifts are very different from that of less luminous Seyferts dominating at lower redshifts, corresponding to their different triggering and fueling mechanisms. However, current measurements of the IRLFs of AGN are not accurate enough to allow a more complete understanding to this by employing the method presented here. Due to this limitation, the conclusions drawn here need to be tested further when better measurements of IRLFs are available.

More accurate measurements of the IRLFs of AGN, especially those determined at smaller redshift bins and more accurately separated to that for type-1 and type-2, are very helpful for a more complete understanding of the evolution of LFs and obscuration of AGN. Based on the observations of newly launched IR space telescope such as *Spitzer*, *Herschel* and forthcoming *James Webb Space Telescope (JWST)*, better measurements of the IRLFs of AGN are expected. These measurements will largely improve our understanding of the evolution of LFs and obscuration of AGN and their co-evolution with galaxies.

ACKNOWLEDGMENTS

We appreciate the anonymous referee for reviewing our paper very carefully and relevant comments on our work. We thank the previous anonymous referee for his/her comments and suggestions that largely improved this paper. This work is supported by the National Natural Science Foundation of China (Grant Nos. 10778702, 11033008, 11063003 and 11103072), the National Basic Research Program of China (Grant No. 2009CB824800) and the Chinese Academy of Sciences (Grant No. KJCX2-YW-T24).

REFERENCES

Aird J. et al., 2010, MNRAS, 401, 2531
Alonso-Herrero A., Quillen A. C., Simpson C., Efstathiou A., Ward M. J., 2001, AJ, 121, 1369
Antonucci R., 1993, ARA&A, 31, 473
Babbedge T. S. R. et al., 2006, MNRAS, 370, 1159
Bahcall J. N., Kirhakos S., Saxe D. H., Schneider D. P., 1997, ApJ, 479, 642
Baldwin J. A., Phillips M. M., Terlevich R., 1981, PASP, 93, 5
Ballantyne D. R., 2008, ApJ, 685, 787
Ballantyne D. R., Everett J. E., Murray N., 2006a, ApJ, 639, 740
Ballantyne D. R., Shi Y., Rieke G. H., Donley J. L., Papovich C., Rigby J. R., 2006b, ApJ, 653, 1070
Barcons X. et al., 2007, A&A, 476, 1191
Barger A. J., Cowie L. L., Mushotzky R. F., Yang Y., Wang W.-H., Steffen A. T., Capak P., 2005, AJ, 129, 578
Bongiorno A., Zamorani G., Gavignaud I., Marano, 2007, A&A, 472, 443

Bower R. G., Benson A. J., Malbon R., Helly J. C., Frenk C. S., Baugh C. M., Cole S., Lacey C. G., 2006, MNRAS, 370, 645
Brown M. J. I. et al., 2006, ApJ, 638, 88
Brusa M. et al., 2010, ApJ, 716, 348
Canalizo G., Stockton A., 2001, ApJ, 555, 719
Cirasuolo M., Magliocchetti M., Celotti A., 2005, MNRAS, 357, 1267
Croom S. M., Smith R. J., Boyle B. J., Shanks T., Miller L., Outram P. J., Loaring N. S., 2004, MNRAS, 349, 1397
Croton D. J. et al., 2006, MNRAS, 365, 11
Davies R. I. et al., 2006, ApJ, 646, 754
Di Matteo T., Springel V., Hernquist L., 2005, *Nature*, 433, 604
Di Matteo T., Colberg J., Springel V., Hernquist L., Sijacki D., 2008, ApJ, 676, 33
Disney M. J. et al., 1995, Nat, 376, 150
Draper A. R., Ballantyne D. R., 2011, ApJ, 729, 109
Ebrero J. et al., 2009, A&A, 493, 55
Fan X. et al., 2001, AJ, 121, 54
Ferland G., Korista K., Verner D., Ferguson J., Kingdon J., Verner E., 1998, PASP, 110, 761
Ferrarese L., Merritt D., 2000, ApJ, 539, L9
Fontanot F., Cristiani S., Monaco P., Nonino M., Vanzella E., Brandt W. N., Grazian A., Mao J., 2007, A&A, 461, 39
Fu H. et al., 2010, ApJ, 722, 653
Gandhi P., Horst H., Smette A., Hönig S., Comastri A., Gilli R., Vignali C., Duschl W., 2009, A&A, 502, 457
Gebhardt K. et al., 2000, ApJ, 539, L13
Gilli R., Comastri A., Hasinger G., 2007, A&A, 463, 79
Goulding A. D., Alexander D. M., 2009, MNRAS, 398, 1165
Graham A. W., 2004, ApJ, 613, L33
Grogin N. A. et al., 2005, ApJ, 627, L97
Gültekin K. et al., 2009, ApJ, 698, 198
Hao L. et al., 2005, AJ, 129, 1795
Häring N., Rix H.-W., 2004, ApJ, 604, L89
Hasinger G., 2004, NuPhS, 132, 86
Hasinger G., 2008, A&A, 490, 905
Hasinger G., Miyaji T., Schmidt M., 2005, A&A, 441, 417
Hönig S. F., Kishimoto M., 2010, A&A, 523, A27
Hönig S. F., Beckert T., Ohnaka K., Weigelt G., 2006, A&A, 452, 459
Hönig S. F., Kishimoto M., Gandhi P., Smette A., Asmus D., Duschl W., Polletta M., Weigelt G., 2010, A&A, 515, A23
Hopkins A. M., 2004, ApJ, 615, 209
Hopkins P. F., Richards G. T., Hernquist L., 2007, ApJ, 654, 731
Hopkins P. F., Hernquist L., Cox T. J., Di Matteo T., Martini P., Robertson B., Springel V., 2005, ApJ, 630, 705
Hopkins P. F., Somerville R. S., Hernquist L., Cox T. J., Robertson B., Li Y., 2006, ApJ, 652, 864
Hopkins P. F., Hernquist L., Cox T. J., Robertson B., Krause E., 2007, ApJ, 669, 67
Hopkins P. F., Hernquist L., Cox T. J., Keres D., 2008, ApJ, 175, 356
Hopkins P. F., Younger J. D., Hayward C. C., Narayanan D., Hernquist L., 2010, MNRAS, 402, 1693
Horst H., Smette A., Gandhi P., Duschl W. J., 2006, A&A, 457, L17
Horst H., Gandhi P., Smette A., Duschl W. J., 2008, A&A, 479, 389
Hutchings J. B., 1987, ApJ, 320, 122
Jahnke K., Macciò A. V., 2011, ApJ, 734, 92
Kauffmann G. et al., 2003, MNRAS, 346, 1055
Kewley L. J., Dopita M. A., Smith H. A., 2001, In Bulletin of the American Astronomical Society, volume 33 of *Bulletin of the American Astronomical Society*, 1365
Kewley L. J., Groves B., Kauffmann G., Heckman T., 2006, MNRAS, 372, 961
Khachikian E. Y., Weedman D. W., 1974, ApJ, 192, 581
Kirhakos S., Bahcall J. N., Schneider D. P., Kristian J., 1999, ApJ, 520, 67
Kormendy J., Bender R., 2009, ApJ, 691, L142
Kormendy J., Richstone D., 1995, ARA&A, 33, 581
Krabbe A., Boker T., Maiolino R., 2001, ApJ, 557, 626
Krolik J. H., 1999, Active galactic nuclei : from the central black hole to the galactic environment. Princeton Univ. Press, Princeton, NJ
Kuraszkiewicz J. K. et al., 2003, ApJ, 590, 128
La Franca F. et al., 2005, ApJ, 635, 864
Laurikainen E., Salo H., 1995, A&A, 293, 683
Liu Y., Zhang S. N., 2011, ApJ, 728, L44
Lutz D., Maiolino R., Spoon H. W. W., Moorwood A. F. M., 2004, A&A, 418, 465
Magorrian J. et al., 1998, AJ, 115, 2285
Maiolino R., Rieke G. H., 1995, ApJ, 454, 95
Marconi A., Hunt L. K., 2003, ApJ, 589, L21
Marconi A., Risaliti G., Gilli R., Hunt L. K., Maiolino R., Salvati M., 2004, MNRAS, 351, 169
Matt G. et al., 1997, A&A, 325,
Matute I., La Franca F., Pozzi F., Gruppioni C., Lari C., Zamorani G., 2006, A&A, 451, 443
Merloni A., 2004, MNRAS, 353, 1035
Merloni A. et al., 2010, ApJ, 708, 137
Miyaji T., Hasinger G., Schmidt M., 2000, A&A, 353, 25
Miyaji T., Hasinger G., Schmidt M., 2001, A&A, 369, 49
Moran E. C., Filippenko A. V., Chornock R., 2002, ApJ, 579, L71
Mullaney J. R., Alexander D. M., Goulding A. D., Hickox R. C., 2011, MNRAS, 414, 1082
Nagar N. M., Falcke H., Wilson A. S., 2005, A&A, 435, 521
Nenkova M., Ivezić Ž., Elitzur M., 2002, ApJ, 570, L9
Nenkova M., Sirocky M. M., Ivezić v. Z., Elitzur M., 2008a, ApJ, 685, 147
Nenkova M., Sirocky M. M., Nikutta R., Ivezić v. Z., Elitzur M., 2008b, ApJ, 685, 160
Netzer H., Mainieri V., Rosati P., Trakhtenbrot B., 2006, A&A, 453, 525
Netzer H. et al., 2007, ApJ, 666, 806
Peng C. Y., 2007, ApJ, 671, 1098
Pier E. A., Krolik J. H., 1992, ApJ, 401, 99
Richards G. T. et al., 2006, AJ, 131, 2766
Rigby J. R., Rieke G. H., Donley J. L., Alonso-Herrero A., Perez-Gonzalez P. G., 2006, ApJ, 645, 115
Risaliti G., Elvis M., Nicastro F., 2002, ApJ, 571, 234
Risaliti G., Maiolino R., Salvati M., 1999, ApJ, 522, 157
Risaliti G., Elvis M., Fabbiano G., Baldi A., Zezas A., 2005, ApJ, 623, L93
Rowan-Robinson M., 1977, ApJ, 213, 635
Schmitt H. R., 2001, AJ, 122, 2243
Shankar F., Mathur S., 2007, ApJ, 660, 1051
Silverman J. D. et al., 2005a, ApJ, 624, 630
Silverman J. D. et al., 2005b, ApJ, 618, 123
Silverman J. D. et al., 2008, ApJ, 679, 118
Simpson C., 2005, MNRAS, 360, 565
Spergel D. N. et al., 2003, ApJS, 148, 175
Steffen A. T., Barger A. J., Cowie L. L., Mushotzky R. F., Yang Y., 2003, ApJ, 596, L23

Steffen A. T., Strateva I., Brandt W. N., Alexander D. M., Koekemoer A. M., Lehmer B. D., Schneider D. P., Vignali C., 2006, AJ, 131, 2826
Tozzi P. et al., 2006, A&A, 451, 457
Treister E., Urry C. M., 2006, ApJ, 652, L79
Treister E. et al., 2004, ApJ, 616, 123
Treister E. et al., 2006, ApJ, 640, 603
Treister E., Natarajan P., Sanders D. B., Urry C. M., Schawinski K., Kartaltepe J., 2010, Science, 328, 600
Tremaine S. et al., 2002, ApJ, 574, 740
Ueda Y., Akiyama M., Ohta K., Miyaji T., 2003, ApJ, 598, 886
Vagnetti F., Turriziani S., Trevese D., Antonucci M., 2010, A&A, 519, A17
Wang J. M., Zhang E. P., 2007, ApJ, 660, 1072
Wang J.-M., Zhang E.-P., Luo B., 2005, ApJ, 627, L5
Wolf C., Wisotzki L., Borch A., Dye S., Kleinheinrich M., Meisenheimer K., 2003, A&A, 408, 499
Yencho B., Barger A. J., Trouille L., Winter L. M., 2009, ApJ, 698, 380
Zhang E. P., Wang J. M., 2006, ApJ, 653, 137
Zhang S. N., 2004, ApJ, 618, L79